9498 *Biochemistry* **2010,** *49,* 9498–9507
DOI: 10.1021/bi1013886

BIOCHEMISTRY
including biophysical chemistry & molecular biology
Article

Phospholipid Hydrolysis Caused by *Clostridium perfringens* α-Toxin Facilitates the Targeting of Perfringolysin O to Membrane Bilayers[†]

Paul C. Moe and Alejandro P. Heuck*

Department of Biochemistry and Molecular Biology, University of Massachusetts, Amherst, Massachusetts 01003, United States

Received August 27, 2010; Revised Manuscript Received September 30, 2010

ABSTRACT: *Clostridium perfringens* causes gas gangrene and gastrointestinal disease in humans. These pathologies are mediated by potent extracellular protein toxins, particularly α-toxin and perfringolysin O (PFO). While α-toxin hydrolyzes phosphatidylcholine and sphingomyelin, PFO forms large transmembrane pores on cholesterol-containing membranes. It has been suggested that the ability of PFO to perforate the membrane of target cells is dictated by how much free cholesterol molecules are present. Given that *C. perfringens* α-toxin cleaves the phosphocholine headgroup of phosphatidylcholine, we reasoned that α-toxin may increase the number of free cholesterol molecules in the membrane. Our present studies reveal that α-toxin action on membrane bilayers facilitates the PFO−cholesterol interaction as evidenced by a reduction in the amount of cholesterol required in the membrane for PFO binding and pore formation. These studies suggest a mechanism for the concerted action of α-toxin and PFO during *C. perfringens* pathogenesis.

Clostridial myonecrosis or gas gangrene, a fulminant human infection inflicted by several Gram-positive *Clostridium* species, promotes a painful and fast destruction of healthy tissue if not properly treated with antibiotics. *Clostridium perfringens* type A is the most common bacterium isolated from patients presenting trauma-induced gas gangrene. Analysis of infected tissues shows edema, thrombosis, and restriction of leukocyte infiltration to the perivascular regions in the infected site. This complex pathology is mediated by potent extracellular protein toxins, especially α-toxin (a phospholipase C) and θ-toxin (perfringolysin O or PFO)[1] (*1*). While α-toxin hydrolyzes phosphatidylcholine (PC) and sphingomyelin (SM), PFO forms large transmembrane pores on cholesterol-containing membranes. Of the several exotoxins produced by *C. perfringens*, only α-toxin and PFO have been implicated in pathogenesis (*2*).

α-Toxin is essential for growth and spread of infection in the host (*3*), and it helps *C. perfringens* avoid the host defense mechanism by altering the normal traffic of the host phagocytes (*4*, *5*). The role played by α-toxin in pathogenesis is dictated by its ability to interact with membranes, whether from outside the cell or while inside the phagosomes (*6*).

PFO is the prototypic member of the cholesterol-dependent cytolysin (CDC) family that includes listeriolysin O (LLO), streptolysin O (SLO), pneumolysin, and others (*7*−*9*). The CDC are β-barrel pore-forming toxins that are secreted by the bacterium as monomeric water-soluble proteins (*10*). Upon encountering a cholesterol-containing membrane (*11*−*14*), PFO monomers bind (*15*, *16*), oligomerize, and form ring-like structures (*17*, *18*), that ultimately insert a large β-barrel into the membrane (*19*−*22*). Despite the progress made in understanding the molecular mechanism of PFO cytolysis (*14*, *15*, *23*, *24*), the importance of PFO in the development and progression of *C. perfringens* gas gangrene is less well understood. Interestingly, it has been shown that PFO and α-toxin exhibit a synergic effect in the establishment of the infection and development of gangrene (*1*, *3*, *25*).

We have shown that PFO binding to model membranes requires a relatively high concentration of cholesterol (*16*, *26*), and the ability of PFO to puncture the membrane seems to be dictated by how much free cholesterol is present in the lipid bilayer (*11*, *27*−*30*). Similar effects were observed for the activity of cholesterol oxidase (*31*−*33*), the rate of sterol transfer by β-methylcyclodextrin (*34*−*37*), and the activation of SREBP-2 on the endoplasmic reticulum (*38*).

The enzymatic activity of *C. perfringens* α-toxin generates diacylglycerol by releasing the phosphocholine headgroup of PC. Therefore, we reasoned that α-toxin activity may increase the amount of free cholesterol in the membrane and assist the interaction of PFO with the cell membranes (see Figure 4 below) (*31*). This is noteworthy because certain CDCs have been reported to act on intracellular membranes which may not ordinarily contain enough cholesterol to trigger toxin binding (*39*−*42*).

Our present studies revealed that α-toxin action on membrane bilayers triggers PFO binding even in membranes containing low cholesterol levels. These studies suggest a mechanism for the concerted action of α-toxin and PFO during *C. perfringens* pathogenesis: the α-toxin activity facilitates the exposure of free cholesterol molecules, sensitizing the cell membrane for PFO binding and cytolysis.

EXPERIMENTAL PROCEDURES

Preparation of PFO Derivatives. The expression and purification of the PFO derivatives were done as described previously (*11*, *15*, *20*, *29*). The PFO derivative containing the native sequence (amino acids 29−500) plus the polyhistidine tag

[†]This work was supported in part by an award from the American Heart Association to A.P.H.

*Corresponding author. Phone: (413) 545-2497. Fax: (413) 545-3291. E-mail: heuck@biochem.umass.edu.

[1]Abbreviations: PFO, perfringolysin O; CDCs, cholesterol-dependent cytolysins; LLO, listeriolysin O; POPC, 1-palmitoyl-2-oleoyl-*sn*-glycero-3-phosphocholine; POPE, 1-palmitoyl-2-oleoyl-*sn*-glycero-3-phosphoethanolamine; DAG, 1-palmitoyl-2-oleoyl-*sn*-glycerol; GSH, reduced L-glutathione; OG, Oregon Green-488X; Fl, fluorescein; PC, phosphatidylcholine; PI, phosphatidylinositol; SM sphingomyelin; DTT, (2*S*,3*S*)-1,4-bissulfanylbutane-2,3-diol; EDTA, ethylenedinitrilotetraacetic acid; D4, domain 4; DPA, dipicolinic acid.

 Published on Web 10/01/2010

that came from the pRSETB vector (Invitrogen) is named nPFO. The Cys-less derivative of nPFO (where Cys459 was replaced by Ala) is named rPFO. Since no significant functional or structural differences were found between PFO derivatives bearing or lacking the polyhistidine tag, the nPFO and rPFO derivatives were used in this study directly as purified (*11*).

Preparation of Lipids and Liposomes. Nonsterol lipids were obtained from Avanti Polar Lipids (Alabaster, AL), and cholesterol was from Steraloids (Newport, RI). Large unilamellar vesicles were prepared with mixtures of 1-palmitoyl-2-oleoyl-*sn*-glycero-3-phosphocholine (POPC), 1-palmitoyl-2-oleoyl-*sn*-glycero-3-phosphoethanolamine (POPE), 1-palmitoyl-2-oleoyl-*sn*-glycerol (DAG), or cholesterol (5-cholesten-3β-ol) and were generated as described previously (*43*). Briefly, chloroform solutions of the lipids were combined, shell-dried under nitrogen, rehydrated at ~21−23 °C in buffer A (50 mM HEPES, 100 mM NaCl, pH 7.5) to 5−30 mM final concentration of total lipids (final volume 0.5 mL), and extruded through 0.1 μm polycarbonate filters (Avanti Polar Lipids) (*44*). Reduced L-glutathione (GSH) was labeled with 5-iodoacetamidofluorescein (Fl; Molecular Probes, Invitrogen) by incubating a 1:1 molar ratio mixture in buffer A for 18 h and stored at −20 °C until use. β-Amylase was labeled with the succinimidyl ester of Oregon Green-488X, 6-isomer (OG; Molecular Probes, Invitrogen) by incubating a 1:1 molar ratio mixture in 100 mM sodium bicarbonate, pH 8.3. Liposomes encapsulating terbium dipicolinic acid [$Tb(DPA)_3^{3-}$], GSH-Fl, or β-amylase OG were prepared as described previously (*43*).

Assay for PFO Binding. For the spectroscopic analysis of PFO−membrane interactions, 288 μL aliquots of 200 nM purified PFO in buffer A were distributed into quartz microcells. After measuring the initial net (after blank subtraction) fluorescence intensity (F_{sol}) of each sample, each cuvette received 12 μL of 5 mM liposomes (total lipid) to a final concentration of 200 μM. The PFO−liposome samples were mixed and incubated at 37 °C for 30 min. After equilibration to 25 °C, the net (after blank subtraction and dilution correction) emission intensity (F_{memb}) of each sample was measured. The change in the Trp emission intensity produced by the binding of PFO to cholesterol-containing membranes was expressed as F_{memb}/F_{sol} (*11*, *16*, *29*, *43*).

Assay for Pore Formation. Pore formation was determined using liposomes loaded with GSH-Fl, or β-amylase-OG, and an anti-fluorescein antibody added to the external buffer solution as a quencher (*43*). Liposomes (50 μM total lipids) were suspended in buffer A containing 5 mM $CaCl_2$ and 10 μL of a 1:10 diluted (in buffer A) solution of anti-fluorescein antibody (0.5 μL of this rabbit polyclonal IgG fraction quenches ~95% of the emission intensity of 0.8 fmol of GSH-Fl in buffer A; lot 84B1, Molecular Probes, Invitrogen). After thermal equilibration of the liposomes at 37 °C, a background signal was recorded for 5 min, and *C. perfringens* α-toxin (type XIV; Sigma, St. Louis, MO) was added to a final concentration of 0.5 unit/mL (1.4 mg/mL, final volume 1.6 mL). The signal was continuously recorded, and after 15 min of incubation, PFO and ethylenedinitrilotetraacetic acid (EDTA) in buffer A were added to a final concentration of 300 nM and 10 mM, respectively. The PFO-dependent release of the encapsulated GSH-Fl was recorded for an additional 10 min. An identical sample was analyzed, but an equivalent volume of buffer A was added instead of α-toxin (control). Emission intensities were integrated for 5 s at intervals of 30 s and recorded. The net emission intensity (F) of the sample at each time point was determined after dilution correction. The GSH-Fl quenched by the antibody was plotted as (F/F_0), where F is the intensity at any time t, and F_0 is the initial intensity of the liposomes. The maximal quenching (F/F_0) for GSH-Fl under these experimental conditions is typically 0.12 (*43*). Blank measurements were made using an otherwise identical sample that lacked α-toxin and PFO.

Steady-State Fluorescence Spectroscopy. Intensity measurements were performed using a SLM-8100 spectrofluorometer as described earlier (*20*) or a Fluorolog 3-21 spectrofluorometer equipped with a 450 W xenon arc lamp, a double excitation monochromator, a single emission monochromator, and a cooled PMT. Unless otherwise indicated, samples were equilibrated to 25 °C before fluorescence determinations. The excitation wavelength and band-pass and the emission wavelength and band-pass, respectively, were 295, 2, 348, and 4 nm for Trp; 495, 2, 520, and 2 nm for fluorescein; and 492, 2, 518, and 4 for OG. End-point measurements were done in 4 × 4 mm quartz microcells (*43*). When additions were made to microcells, the contents were mixed thoroughly with a 2 × 2 mm magnetic stirring bar as described previously (*45*). Kinetics measurements were done using 1 × 1 cm quartz cells, and the samples were continuously stirred using a magnetic stirring bar (1.5 × 8 mm) (*43*).

For emission spectra determination, aliquots of 2 mL of each PFO derivative were dialyzed simultaneously against 4 L of buffer A supplemented with 1 mM (2*S*,3*S*)-1,4-bissulfanylbutane-2,3-diol (DTT) and 0.5 mM EDTA at 4 °C for 10 h and clarified by centrifugation at 21000*g* for 10 min at 4 °C. After dialysis samples were diluted in quartz microcells with dialysis buffer to a final concentration of 0.5 μM (final volume 300 μL). Spectra for each of these samples were recorded at 25 °C with the excitation wavelength fixed at 270 nm and a band-pass of 2 nm. The emitted light was collected through a vertically oriented Glan-Thompson polarizer (to account for polarization effects in the emission monochromator) (*46*) and wavelengths were scanned from 280 to 450 nm using a band-pass of 4 nm. The signal was integrated for 1 s at intervals of 1 nm. Three independent spectra were recorded for the sample containing the toxin and for the control sample (dialysis buffer). The emission spectrum of the control sample was subtracted from the spectrum of the equivalent sample containing the toxin, and the blank corrected spectrum was smoothed using a Savitzky-Golay smoothing filter (of degree 2) using a window of 11 points (OriginLab software). Fluorescence emission spectra for Trp residues were recorded similarly, except that the excitation wavelength was set at 297 nm and the emission wavelength was scanned from 305 to 450 nm. Total intensity for each sample was calculated as the sum of the intensities obtained at each wavelength of the scanned spectrum.

Urea Unfolding−Refolding Equilibrium Studies. Unfolding was done by mixing the concentrated protein solutions (9−23 μL) into the urea solution (final volume 300 μL, protein concentration 0.5 μM). Urea concentration was determined by measuring the refractive index of the urea stock solution as described by Pace and Scholtz (*47*). Both solutions contained buffer A supplemented with 1 mM DTT and 0.5 mM EDTA. The proteins were incubated for 12 h at 23−25 °C to reach equilibrium. nPFO refolding was done similarly using a stock solution of the protein in 6 M urea. Trp fluorescence emission spectra were measured at 25 °C in the wavelength range 310−450 nm with an excitation wavelength of 297 nm and excitation and emission band-pass widths of 4 and 8 nm, respectively. Total intrinsic fluorescence emission spectra were measured at 25 °C in the wavelength range 287−450 nm with an excitation wavelength of

Table 1: Fluorescence Emission Maxima and Relative Total Fluorescence Intensity for Commonly Used PFO Derivatives[a]

	λ_{ex} = 270 nm		λ_{ex} = 297 nm	
derivative	λ_{em} max	relative total intensity	λ_{em} max	relative total intensity
nPFO	321.5 ± 0.5	1.00	330.5 ± 0.5	1.0
rPFO	328.5 ± 0.5	1.62 ± 0.04	333.5 ± 0.5	2.0 ± 0.1
pAH21His	328.5 ± 0.5	1.62 ± 0.02	333.0 ± 0.5	2.1 ± 0.1
pRT20	332.5 ± 0.5	1.87 ± 0.03	336.0 ± 0.5	2.4 ± 0.2

[a]The emission fluorescence maxima and relative total intensity are indicated for total aromatic amino acids (λ_{ex} = 270 nm) or selectively for the Trp residues (λ_{ex} = 297 nm). Emission scans were performed and corrected as described in Experimental Procedures. Total intensities were obtained from the area under the curve for the corrected spectra. The average and range for two independent determinations are shown.

274 nm and excitation and emission band-pass widths of 2 and 8 nm, respectively. The signal was integrated for 1 s at intervals of 1 nm. Two independent spectra were averaged to reduce background noise. The magic angle configuration was used (Glan-Thompson prism polarizers in both the excitation, 54.7°, and emission, 0°, beams) to ensure that the intensity was proportional to the total light intensity of the sample and to correct for spectral distortions caused by the monochromators (*46*). All spectra were corrected by subtraction of a spectrum of an equivalent buffer solution at the given urea concentration. The observed average energy of emission (or spectral center of mass $\langle v_p \rangle$) was calculated according to $\langle v_p \rangle = \sum v_i F_i / \sum F$, where F_i stands for the fluorescence emitted at wavenumber v_i (*48*). The corresponding wavelength values in nm ($1/\langle v_p \rangle$) were used to estimate the conformational stability of the proteins (ΔG_{U-F}^{water}), assuming a two-state unfolding model for the PFO monomers (*49*, *50*).

RESULTS

Assessing PFO Wild-Type Binding to Membranes Using Intrinsic Fluorescence. When PFO is secreted from *C. perfringens*, the first 28 amino acids required for protein secretion are cleaved (*51*). Recombinant PFO proteins typically carry a modified N-terminus that contains additional amino acids including a polyhistidine tag and antibody epitope, which extends the native mature sequence by ~30 amino acids. To analyze how the spectroscopic properties of PFO are affected by amino acid modifications, we characterized four commonly used PFO derivatives (Table 1; see Supporting Information): (i) the Cys-less original variant of PFO (named pRT20) (*20*, *52*) which contains 36 additional amino acids at the N-terminus, two of which are aromatic and contribute to the spectroscopic signals of the protein (one Trp and one Tyr) (see ref *11* for sequence details); (ii) the PFO construct without the non-native Trp residue in the N-terminus (named rPFO or pAH21) (*11*, *15*); (iii) the His tag minus derivative generated by enterokinase cleavage of the first 32 amino acids of rPFO, generating a protein that contains aromatic residues identical to the wild-type protein, and only 6 extra amino acids on its N-terminus (pAH21His) (*11*); and (iv) the native-like PFO derivative originated by reintroduction of the Cys459 residue into the rPFO construct (named nPFO or pAH11) (*11*, *15*).

The emission spectrum for the Cys-less rPFO revealed a small red shift of the emission maximum and an increase in the total fluorescence intensity when compared with nPFO (Table 1). Examination of the three-dimensional structure of the PFO monomer (*53*) showed that the thiol group of Cys459 lies close to the aromatic ring of Trp467. This suggests that the red shift in the emission spectrum and higher fluorescence emission intensity observed for rPFO result mainly from the absence of Cys459 and its thiol group which quenches Trp467. The pRT20 derivative showed an additional red shift in the maximum of the emission spectrum, suggesting that the extra Trp in the N-terminus of this derivative is located in a polar environment, presumably exposed to an aqueous environment as expected for a nonstructured segment (*53*).

We have shown previously that the Trp fluorescence change that follows PFO/membrane incubations can be used to quantify toxin binding (*11*). Since the water-soluble forms of PFO employed in our studies differ slightly in their intrinsic fluorescence properties, it is expected that the relative emission intensity change observed upon membrane binding, (F_{memb}/F_{sol}), will differ for different PFO derivatives. Therefore, fluorescence intensities were normalized to directly compare the binding isotherms for different PFO derivatives (see below).

PFO Binding and Pore Formation Have Similar Cholesterol Dependence. Studies using intermedilysin, a CDC that requires cholesterol for pore formation but not for binding, revealed that cholesterol plays multiple roles in the CDC mechanism (*14*). In addition to modulating the binding of PFO, cholesterol also seems to be required for the insertion of the amphipathic β-hairpins. Does PFO pore formation have a different cholesterol threshold than the binding to membranes? Liposomes formed with different mixtures of POPC and cholesterol were used to follow nPFO binding and pore formation as a function of cholesterol content. Binding was followed using the intrinsic Trp fluorescence increment that results from the interaction of PFO domain 4 (D4) with the membrane (Figure 1A, filled symbols) (*11*). For nPFO, membrane binding increases sharply above 35 mol % cholesterol with apparent saturation near 45 mol %. PFO pore formation was detected by the decrease in the fluorescence signal (fraction of GSH-Fl quenched) caused by the specific binding of the antibody to the fluorescein dye (*43*). In good agreement with the binding data, pore formation was minimal at cholesterol levels below 35 mol %. The mid transition to maximal pore formation occurs at 42 mol % cholesterol, just 2 mol % above the mid transition for the binding process. This small effect could be explained by the nonhomogeneous distribution of PFO molecules on liposomes containing slightly different amounts of cholesterol. While some vesicles are punctured by more than one pore, others may not bind enough monomers to trigger the insertion of the β-hairpins (*21*). As observed for the binding measurements, maximal pore formation was reached as cholesterol approaches 50 mol %. We conclude from these data that if there is enough cholesterol to trigger PFO binding, under conditions that do not preclude pore formation (like, for example, low temperature or when using nonlytic PFO variants (*16*, *18*)), pore formation will occur. Thus, the PFO cytolytic mechanism is modulated by cholesterol at the initial binding step.

Enhancing Free Cholesterol Molecules Promotes PFO Binding: Effect of POPE. The appearance of free cholesterol in the membrane is affected by both the total amount of cholesterol present in the membrane and the overall phospholipid composition of the lipid bilayer (*54*). Hence, PFO binding can be modulated by changes in the phospholipid composition, like the length of the phospholipid acyl chains and the degree of acyl chain saturation (*11*, *30*, *55*).

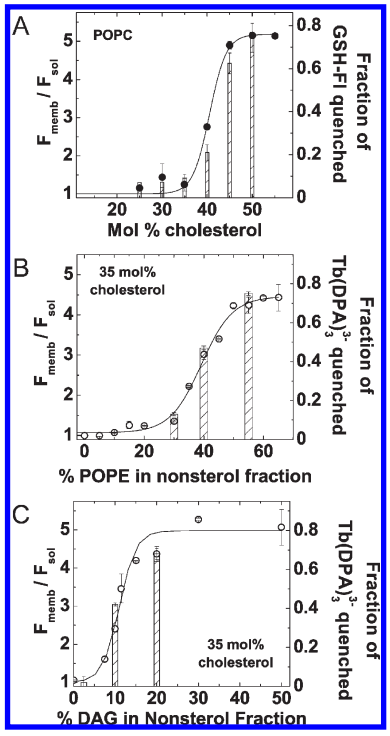

FIGURE 1: Cholesterol dependence of nPFO binding to membranes composed of cholesterol and glycerolipids with different headgroups. nPFO binding to liposomal membranes was followed by the increase in the net Trp emission intensity (F_{memb}/F_{sol}) calculated as described in Experimental Procedures. (A) Binding of nPFO to POPC/cholesterol liposomes (filled circles). The mol % of cholesterol was increased from 25% to 55%. (B) Binding of nPFO to membranes containing a constant 35 mol % cholesterol and different ratios of POPE/POPC, ranging from 0 (no POPE) to 1.9 (open circles). (C) Binding of nPFO to membranes containing 35 mol % cholesterol and different ratios of DAG/POPC ranging from 0 (no DAG) to 1 (open circles). In all panels, pore formation was evaluated using liposomes prepared with selected lipid compositions, and the fraction of fluorophore quenched is indicated using bars. Each data point shows the average of at least two independent measurements and their range.

Appearance of free cholesterol molecules in the membrane is also affected by the headgroup of the phospholipids (*56*). We therefore quantified how much the change of a choline group, for a smaller ethanolamine group, affected PFO binding at a fixed cholesterol concentration. We prepared membranes containing increasing amounts of POPE (by replacing an equal amount of POPC) at a cholesterol concentration fixed at 35 mol % of the total lipids and determined the binding of nPFO. When only POPC is present in membranes containing 35 mol % cholesterol, nPFO does not bind (Figure 1). However, nPFO started to bind when 30% of POPC was replaced by POPE (Figure 1B, POPE, 19.5 mol % of the total lipids). Maximal binding was obtained with an equimolar mixture of POPE/POPC. On the basis of these observations, one would predict that the smaller the headgroup of the phospholipid, the less cholesterol will be required in the membrane to trigger PFO binding. Does the addition of POPE have any effect on pore formation? As observed for just POPC, binding of PFO to POPC/POPE membranes dictates how much pore formation occurs, as determined by the quenching of the encapsulated marker (Figure 1B, bars). No pore formation was detected on membranes containing 5% POPE in the nonsterol lipid fraction, but pore formation paralleled PFO binding to membranes above 30% POPE.

Enhanced Free Cholesterol Exposure Promotes PFO Binding: Effect of DAG. Elimination of the phosphocholine group in POPC, which leaves the glycerol backbone plus both acyl chains, should have a maximal affect on the exposure of free cholesterol molecules and consequent PFO binding. Using a similar approach to that outlined in the previous section, we analyzed the binding of nPFO to liposomes prepared with different amounts of POPC and DAG (Figure 1C, open circles).

Surprisingly, the threshold for PFO binding was abruptly achieved as the membrane population of DAG composes only 5 mol % of the total lipids, with saturation levels reached at approximately 13 mol % DAG. The replacement of small amounts of POPC by DAG was enough to enhance the exposure of free cholesterol molecules and trigger PFO binding. As observed for the analysis of POPE, pore formation paralleled the binding of nPFO at different DAG concentrations (Figure 1C, bars).

The above results confirmed that, at a fixed cholesterol concentration, the smaller the phospholipid head of the added glycerolipid, the lower the threshold for PFO binding. Binding of PFO to membrane bilayers can, therefore, be modulated by the overall lipid composition rather than solely by the total cholesterol content.

Cholesterol Dependence of the Cys-less PFO Mutant rPFO. Most of the structural and mechanistic studies of PFO have been done with a Cys-less derivative rPFO, where the unique and conserved Cys459 was replaced by Ala (*11*, *15*−*17*, *19*−*22*, *29*, *43*). Both nPFO and rPFO have similar hemolytic activity and efficiently bind to liposomes containing high cholesterol (more than 50 mol % cholesterol) (*20*). Based on these observations, it has been commonly assumed that the binding properties of the Cys-less derivatives for some CDCs were the same. However, we noticed that the cholesterol-dependent binding of these two PFO derivatives has different sterol concentration threshold (Figure 2A and Figure 3). The C459A mutant rPFO required ~5 mol % more cholesterol to trigger binding to POPC/cholesterol liposomes as compared with nPFO.

We therefore asked if the C459A mutation affected the conformational stability of the toxin. It was found that, despite causing a small but significant change in the cholesterol-dependent binding properties of PFO, the C459A mutation did not alter the stability of the toxin, as determined by the equilibrium urea denaturation of the monomeric protein (Figure 2C) (*49*, *50*, *57*). nPFO unfolding by urea was reversible, with a $\Delta G_{U-F}^{water} = 11 \pm 3$ kcal mol^{-1} (Figure 2B). The data were fitted assuming a two-state model, and similar results were obtained whether we measured the changes in the average energy of emission (Figure 2B,C) or the total fluorescence intensity under the spectrum (data not shown) (*49*). The whole PFO molecule unfolded cooperatively as indicated by the similar concentration of urea required for 50% unfolding when only Trps were excited at 297 nm (Figure 2B) or when all aromatic amino acids were excited at 274 nm (data not shown). While Trp fluorescence reports mostly the unfolding of D4 (six of the seven Trp residues are located in this domain), excitation at 274 nm reports the unfolding of the overall molecule (23 Tyr residues are distributed all over the molecule; Table S1, Supporting Information).

The change of the conserved Cys459 to Ala affected neither the stability of the PFO molecule nor the activity of PFO at high cholesterol concentration. However, it is clear that this residue contributes to the ability of PFO to interact with cholesterol when the membrane contains lower cholesterol levels.

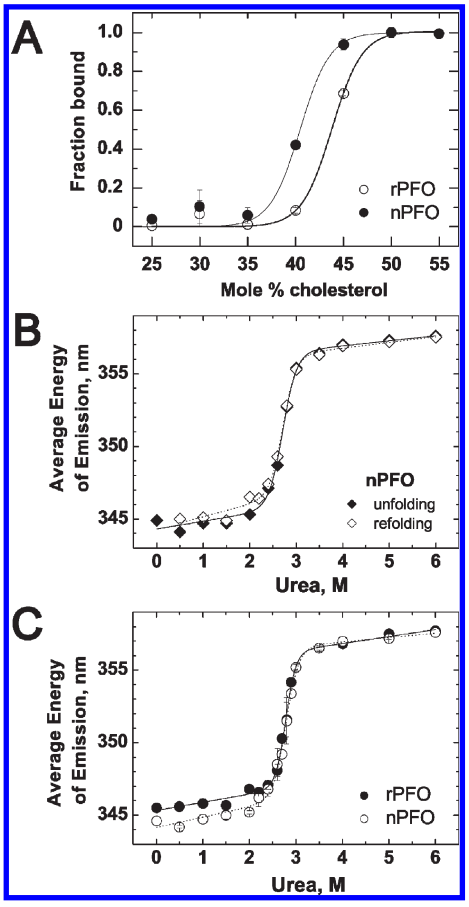

FIGURE 2: Cholesterol-dependent binding and stability of nPFO and rPFO. (A) The fraction of bound rPFO (open circles) is compared with the fraction of bound nPFO (filled circles) to POPC liposomes containing the indicated amount of cholesterol. Measurements were done as indicated in Figure 1 and normalized to account for the difference in the total fluorescence observed for each mutant. (B) Urea denaturation and renaturation of nPFO. The average energy of emission for each fluorescence emission spectrum was obtained for nPFO at given urea concentrations. Samples of nPFO in buffer A or nPFO in 6 M urea in buffer A were added and equilibrated at the indicated urea concentration as described in Experimental Procedures. (C) Urea denaturation for rPFO and nPFO. The average energy of emission for each fluorescence emission spectrum was obtained for nPFO or rPFO at given urea concentrations. The data in (B) and (C) were fitted assuming that the average energy of emission of the folded and unfolded states varies linearly with urea concentration.

C. perfringens α-*Toxin Facilitates PFO Membrane Interaction*. α-Toxin alters the properties of the target cell membrane by removing the phosphocholine moieties from PC and SM. As a consequence of the headgroup removal, more free cholesterol molecules appear in the membrane. Does the α-toxin modification of the membrane facilitate PFO binding and pore formation as a result of the increase in the number of free cholesterol?

PFO binding changes abruptly from no binding to complete binding in a very narrow range of cholesterol concentrations (only a 10 mol % cholesterol increment). To evaluate how α-toxin activity affects the number of free cholesterol molecules present in the membrane, we measured the affect of α-toxin on PFO activity using membranes containing cholesterol concentrations just below the binding threshold. We measured the kinetics of pore formation for both nPFO and rPFO derivatives, on membranes treated, or nontreated, with α-toxin. The extent of PFO pore formation on untreated liposomes (Figure 3, filled symbols) correlated well with the extent of binding observed for these PFO derivatives (Figure 2A).

A baseline signal was measured during 5 min before the addition of α-toxin (Figure 3, open circles) or the addition of an equivalent amount of buffer A (control, Figure 3, filled circles). Some quenching of GSH-Fl was observed during α-toxin incubations. The origin for the GSH-Fl leakage is not known, but it may be caused by the fusion of some vesicles (*58*, *59*) or by nonspecific GSH-Fl leakage through transient disruptions caused by α-toxin. The amount and rate of leakage of GSH-Fl were independent of the cholesterol concentration (Figure 3, open circles, between 5 and 20 min) but dependent on the concentration of α-toxin (Figure 2S, Supporting Information). Similar leakage was observed when a larger reporter, β-amylase-OG (ca. 100 Å vs ca. 10 Å for GSH-Fl), was encapsulated in the liposomes, indicating that both small and large molecules were released and quenched by the anti-Fl/OG-antibody (ca. ~120 Å) (*43*) as a consequence of the α-toxin activity (data not shown).

After 15 min of incubation with α-toxin, PFO and EDTA were simultaneously added (the latter to chelate Ca^{2+} ions and thus inhibit α-toxin) (*60*), and pore formation was followed for an additional 10 min. An increase in the extent of pore formation was observed for both PFO derivatives when membranes containing more than 30 mol % cholesterol were previously exposed to α-toxin (compare open vs filled circles in Figure 3). When only EDTA was added (control with no PFO), no significant change was observed in GSH-Fl quenching (Figure 3E, solid line). The closer the cholesterol concentration approached the threshold required to trigger PFO binding, the more prominent was the effect of α-toxin. In particular for rPFO, note that the extent of pore formation increased more than 3-fold when liposomes containing 40 mol % cholesterol were preincubated with α-toxin (Figure 3F).

In agreement with the data obtained with liposomes prepared with POPE or DAG (Figure 1B,C), hydrolysis of the phosphocholine group from POPC by α-toxin increased the amount of free cholesterol molecules in the membrane and as a consequence facilitated PFO binding and pore formation.

DISCUSSION

Our examination of the cholesterol dependence of PFO binding and pore formation has provided four primary insights into the mechanism of PFO interaction with cholesterol in membrane bilayers. First, cholesterol-dependent PFO pore formation is regulated at the initial binding step of the cytolytic mechanism. Second, the amount of cholesterol required to trigger PFO binding to membranes is reduced when phospholipids with smaller headgroups are present (e.g., DAG or POPE, compared to POPC). Third, the conserved Cys459 is important for cholesterol recognition in membranes containing low cholesterol levels. Fourth, α-toxin activity (i.e., hydrolysis and release of phospholipid headgroups) facilitates PFO cytolytic activity in membranes containing low cholesterol content. In addition, we have determined that the chemical denaturation and refolding of the PFO monomer by urea are reversible processes, with a $\Delta G_{U-F}^{water} = 11 \pm 3$ kcal mol^{-1}.

Cholesterol is essential for PFO cytolysis; however, the exact mechanism for this specific protein−lipid interaction remains elusive (*9*, *61*, *62*). It has become clear that the organization of the cholesterol molecules in the membrane bilayer (*11*, *30*, *56*, *63*) and

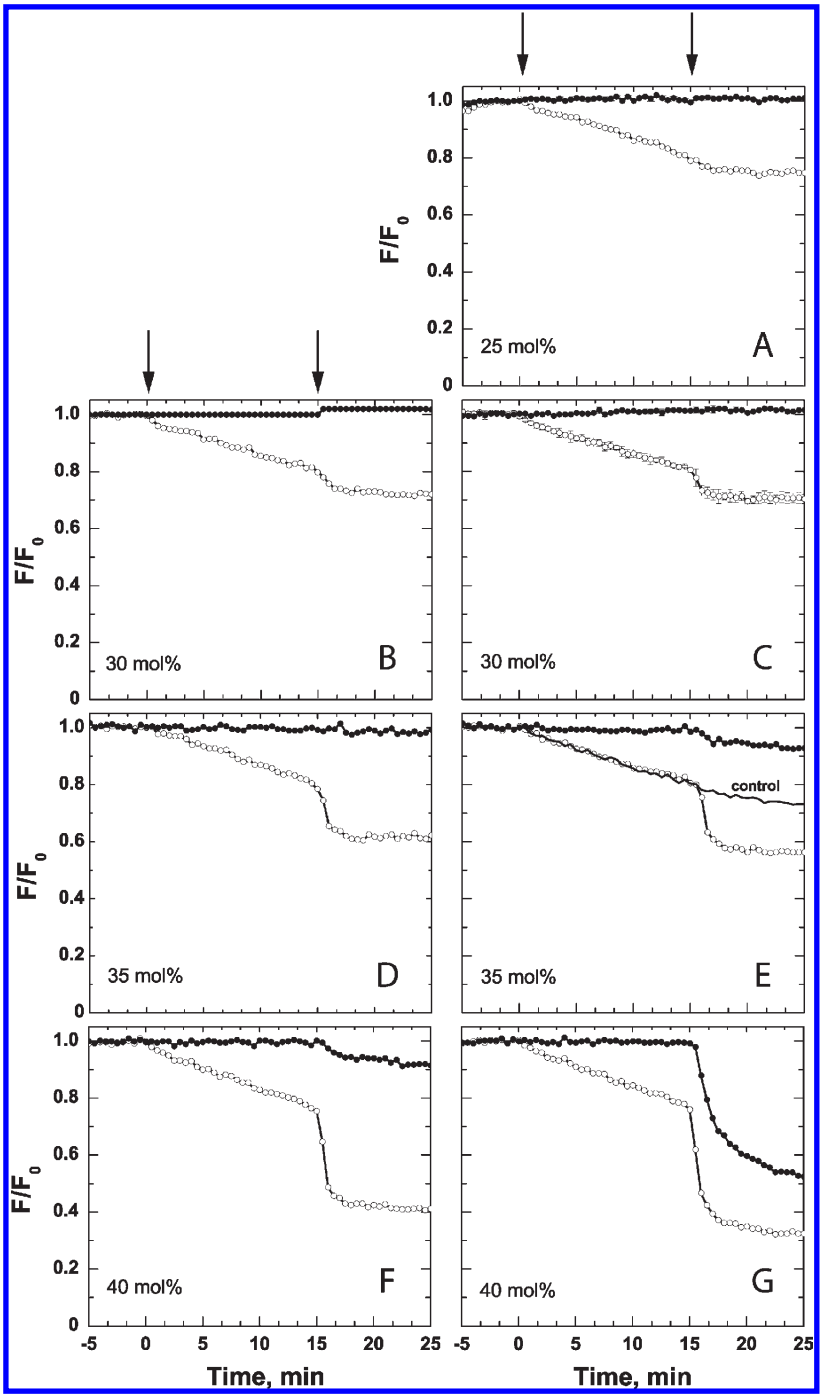

FIGURE 3: *C. perfringens* α-toxin action facilitates PFO−membrane binding and pore formation. Kinetic profiles for the pore formation activity of nPFO (panels A, C, E, G) or rPFO (panels B, D, F) on POPC liposomes containing the indicated amount of cholesterol (mol % of total lipids). Pore formation was determined by the quenching of a liposome-encapsulated GSH-Fl by the externally added anti-Fl antibody as detailed in Experimental Procedures. Liposomes were incubated at 37 °C either with 0.5 unit/mL α-toxin (open circles) or without (control, filled circles) for 15 min whereupon PFO protein was added to a final concentration of 300 nM. Typical error ranges obtained for two independent measurements are shown in panel C. A typical profile for GSH-Fl quenching on liposomes incubated with α-toxin but without addition of PFO is shown in panel E (control). The time of addition of α-toxin and PFO (or equivalent buffer solutions) at 0 and 15 min, respectively, is indicated by the arrows at the top of the panels.

the conformation of the loops located in the tip of PFO D4 play an important role on this interaction (*12*, *13*, *23*).

PFO binds directly to pure cholesterol aggregates in aqueous solutions, but not when cholesterol is complexed with phospholipids or shielded from the membrane surface (Figure 4A) (*16*, *29*, *56*). The minimal amount of cholesterol required to trigger PFO membrane binding is determined by the interactions between the sterol molecules and the phospholipids (*11*, *30*). Less cholesterol is required in the membrane when the liposomes contain unsaturated phospholipids rather than phospholipids with saturated acyl chains. The kinks introduced by the double bonds reduce the area of interaction between the acyl chains and the sterol. Consequently, free cholesterol molecules become more readily available to interact with PFO. In accordance with these observations, molecules that intercalate with the phospholipids but do not interact with PFO move the cholesterol binding threshold to lower cholesterol concentrations (*11*, *64*). A typical binding isotherm for nPFO to POPC membranes prepared with

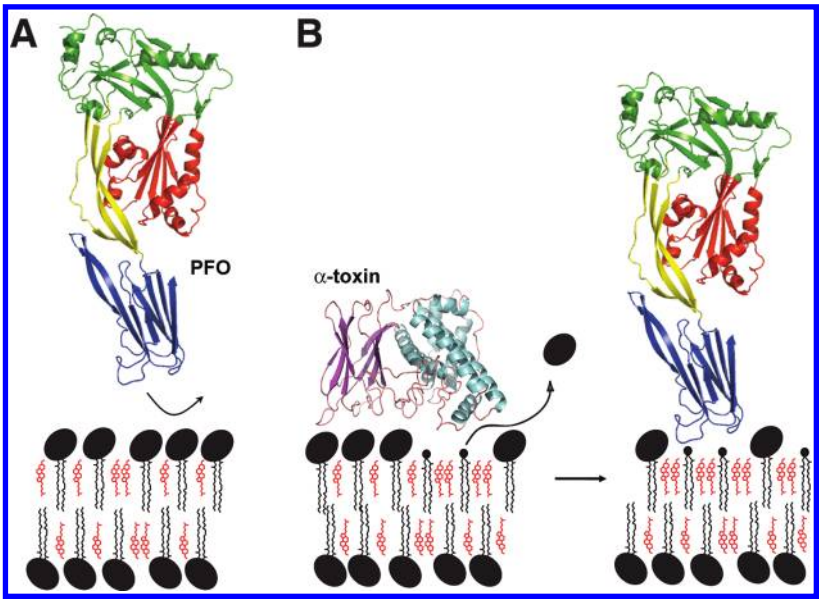

FIGURE 4: A schematic model for the *C. perfringens* α-toxin effect on PFO binding. (A) PFO does not bind to membranes containing low cholesterol content, presumably because no free cholesterol molecules are present in the membrane. (B) *C. perfringens* α-toxin hydrolyzes PC releasing the phosphocholine headgroup and generating DAG. The appearance of free cholesterol molecules triggers D4-mediated PFO binding. PFO and α-toxin cartoon representations were generated using PyMol (Delano Scientific). The phosphocholine headgroup of POPC is represented as a large black oval. The glycerol moiety of DAG is shown as a small black circle.

increasing amounts of cholesterol is shown in Figure 1A. Under these conditions, PFO requires at least 35 mol % cholesterol in the membrane before any binding is detectable (*16*). Once the binding threshold is achieved, there is a relatively narrow range required to reach saturation. This cooperative binding behavior is characteristic of several CDCs like tetanolysin (*65*), SLO (*66*), and LLO (*67*).

Binding of individual PFO monomers to the membrane surface is followed by oligomerization and the formation of the prepore complex (*18*, *43*). The final step of the cytolytic mechanism is the cooperative insertion of two amphipathic β-hairpins per monomer to form a transmembrane β-barrel (*19*, *68*). A comparative analysis between PFO and intermedilysin (a CDC secreted by *Streptococcus intermedius*) showed that the initial and final steps of the cytolytic mechanism are sensitive to the total cholesterol content in the bilayer (*14*). To investigate how cholesterol affects each of these steps, both binding and pore formation were measured using membranes with identical lipid composition. As shown in Figure 1, no significant differences were observed for the binding and the pore formation activity of PFO. The small difference observed between binding and pore formation can be explained by a nonheterogeneous distribution of PFO among the vesicles or, alternatively, by the presence of a small number of noninserted incomplete oligomers. Hence, we concluded that the initial step of the cytolytic mechanism (i.e., cholesterol-dependent binding) determines the ability of PFO to form pores in membranes. What membrane factors affect the PFO−membrane interaction?

Both acyl chain length and saturation have been argued to vary the amount of free cholesterol molecules in the membrane (*37*), thus affecting PFO binding. As suggested for SLO (*56*), we reasoned that structural changes in the phospholipid headgroups could likewise affect cholesterol distribution and therefore toxin binding (*69*). We therefore quantified the effect of the headgroups on PFO binding using membranes containing low cholesterol levels. Maintaining the cholesterol concentration constant at 35 mol % of the total lipids, we gradually replaced some of the POPC content by POPE, and PFO binding was observed only when the POPE/POPC ratio was higher than 1/3, with apparent saturation achieved at equimolar concentrations (Figure 1B). The acyl chains of POPE are identical to those of POPC; thus any effect on the PFO−cholesterol interaction would be a result of the different headgroup. A parsimonious explanation for these data is that the comparatively diminutive ethanolamine headgroup provides less shielding bulk for the cholesterol molecule (*28*, *56*). Alternatively, this observation can also be explained if POPE does not associate as effectively with cholesterol as POPC does, and therefore the amount of free cholesterol molecules increases, as reflected by the boost in the binding of the PFO molecules to the bilayer (*35*). At this point we cannot rule out the possibility that microheterogeneities may exist in the lipid mixtures at high cholesterol concentrations that may also explain the observed binding behavior, like the presence of undetectable nanodomains or cholesterol crystals (*70*, *71*).

Are there any processes that may affect the phospholipid headgroup distribution during *C. perfringens* pathogenesis? *C. perfringens* α-toxin is a phospholipase C which cleaves the headgroup from POPC leaving a DAG moiety in the membrane, certainly the sparest form of a diacyl lipid (Figure 4B). Since the removal of the phospholipid headgroup will increase the amount of free cholesterol in the membrane, we quantified the effect of replacing POPC for DAG on PFO binding. POPC liposomes with 35 mol % cholesterol were used as for the analysis of POPE. POPC was substituted by DAG in a stepwise fashion. Interestingly, the binding threshold was reached when DAG constituted just 5 mol % of the total lipids. Binding saturation was reached when DAG concentration was ~13 mol % of the total lipids (i.e., DAG/POPC ratio of 1/5). When the above experiments were repeated but with liposomes containing 25 mol % cholesterol, a concentration far below the binding threshold level, PFO binding was nevertheless educed when DAG/POPC ratio was higher than 1/3 (data not shown). This effect clearly echoes observations with POPE with the attendant rationale: free cholesterol molecules become available for PFO binding. Is the availability of free

cholesterol the only requisite to trigger PFO binding? Does the conserved Cys play any role in cholesterol recognition?

The tip of PFO D4 contains regions of conservation that suggest a vital role for this domain. A conserved undecapeptide was found to be very important for PFO activity and binding (*72*), and it has long been suggested that this segment may constitute the binding site for a cholesterol molecule (*73*). However, it has been recently implied that the PFO undecapeptide is uncoupled from toxin membrane binding (*12*). Instead, the Thr490 and Leu491 residues located in D4/loop 1 of PFO appear to mediate PFO binding to membranes containing high cholesterol (*23*). Interestingly, we report here that the cholesterol binding properties of the undecapeptide C459A mutant differ from that observed for the native form of PFO. While the mutation affected neither the conformational stability of PFO (Figure 2C) nor the PFO binding at high cholesterol concentration (*20*, *74*−*77*), elimination of the thiol group at residue 459 elevated the binding threshold for cholesterol by 5 mol % (Figure 2A). This observation suggests that binding of PFO to cholesterol-containing membranes may not be completely independent of the conserved undecapeptide. This segment may be important not only for the insertion of the β-hairpins (*12*) but also to modulate how much cholesterol is required on the membrane to trigger binding. The role of the Cys may be critical when the CDCs act on membranes containing low cholesterol levels, as has been suggested for LLO (*78*).

The concentration of cholesterol in human red blood cells is approximately 45 mol % of the total lipid (*79*), and these cells are frequently used to evaluate the activity of different PFO derivatives (*20*, *76*, *80*). It is worth to notice that the cholesterol content of red blood cells is 7−10 mol % higher than the cholesterol content of macrophages (*81*), cells that are a physiological target for PFO. While the C459A mutation may not significantly affect the binding to red blood cells, it may affect the binding to other cells (or to intracellular membranes) that contain lower cholesterol levels.

PFO is secreted by *C. perfringens* to the extracellular medium as an unfolded polypeptide (*51*, *82*). Outside the cell, the toxin spontaneously folds into a rod-shaped molecule with three discontinuous domains (domains 1−3) and a compact C-terminal β-sandwich (or D4, residues 391−500; see Figure 4A) (*53*). Our urea denaturation studies showed that the protein refolds *in vitro* after dilution of the denaturing agent (Figure 2B), accordingly with the spontaneous tendency of the polypeptide to adopt its three-dimensional structure. The free energy of unfolding in water was 11 ± 3 kcal mol^{-1}, assuming a two-state transition for the unfolding equilibrium of the toxin. No significant differences were found in the conformational stability of the rPFO derivative, where the conserved Cys459 was mutated to Ala, when compared with the native-like nPFO derivative. The similarity among the thermodynamic parameters of the two PFO derivatives suggests that no major conformational changes are introduced by this mutation.

Pathogenesis by *C. perfringens* is mediated by two potent exotoxins: α-toxin and PFO. While active individually, it has been shown that they exert a synergic effect during *C. perfringens* infections (*25*, *40*, *83*). Could α-toxin hydrolysis of phospholipids facilitate the cholesterol-dependent interaction of PFO with the membrane? To determine whether the α-toxin activity will increase the amount of free cholesterol in the membrane, and a concomitant increase in PFO binding, membranes containing different amounts of cholesterol were treated with α-toxin and subsequently exposed to PFO. We found that even at cholesterol levels below the usual binding threshold α-toxin preincubation appears to poise membranes for PFO lysis (Figure 3).

Our results revealed that the effect of α-toxin was more pronounced at cholesterol concentrations just below the binding threshold (Figure 3D−F). No significant effect was observed on membranes containing 25 mol % cholesterol (Figure 3A). The lack of synergism at low cholesterol concentrations could be explained by the rapid flip-flop movement of the cholesterol molecules across the membrane bilayer. Free cholesterol molecules generated on the outer leaflet of the bilayer will rapidly equilibrate and form complexes with the excess of phospholipids still present in the inner leaflet of the bilayer (*36*). This is in contrast to the DAG titration experiments (Figure 1C), where the DAG molecules were equally distributed in both leaflets of the bilayer. Thus, observations from the DAG titration experiments appear to have a biological parallel with the lipolytic degradation of POPC by α-toxin with subsequent sensitization to PFO binding and pore formation. These results suggest that the basis of α-toxin and PFO synergy lies in the augment of free cholesterol molecules present in the membrane (Figure 4).

In summary, the data presented here reveal that α-toxin activity facilitates PFO cytolysis on membranes that contain low cholesterol levels. In addition, we showed that the binding threshold for cholesterol can be modulated by modifications in the undecapeptide. These polypeptides are highly conserved among the CDCs (*9*), and their interaction with the membrane may be modulated by changes in the pH of the medium (*30*, *67*). We speculate that these effects are responsible for the activity of CDCs on intracellular membranes, which contain much less cholesterol than the plasma membrane (*84*). Interestingly, both PFO and α-toxin have been reported to be important for the *C. perfringens* escape from the phagosome (*39*, *40*), and both toxins have optimal activity at a mildly acidic pH (*30*, *85*).

It is also important to note that LLO, a CDC secreted by *Listeria monocytogenes*, is essential for the phagosomal escape of this pathogen (*41*, *42*). Interestingly, LLO and two phospholipases (PI-PLC and PC-PLC) are required to effectively dissolve the double-membrane spreading vacuole and evade host-cell defense mechanisms (*86*−*89*). The action of these phospholipases may increase the amount of free cholesterol in the membrane and trigger LLO binding and pore formation in cellular vacuoles, even at a suboptimal pH (*67*). Hence, the results reported here are not limited to *C. perfringens* pathogenesis, and they may be generally applicable to the pathogenic mechanisms of other bacteria, as well as other cellular processes where the action of phospholipases may be coupled to cholesterol-dependent protein−membrane interactions (*90*).

SUPPORTING INFORMATION AVAILABLE

Effect of the time of preincubation with α-toxin on the PFO pore formation activity; effect of the concentration of α-toxin on the sensitization of liposomes to PFO pore formation; list of aromatic residues present in each PFO derivative, molar absorptivity values for each PFO derivative, and the absorption λ_{max} for each PFO derivative. This material is available free of charge via the Internet at http://pubs.acs.org.

REFERENCES

1. Hickey, M. J., Kwan, R. Y. Q., Awad, M. M., Kennedy, C. L., Young, L. F., Hall, P., Cordner, L. M., Lyras, D., Emmins, J. J., and

Rood, J. I. (2008) Molecular and cellular basis of microvascular perfusion deficits induced by *Clostridium perfringens* and *Clostridium septicum*. *PLoS Pathogens 4*, e1000045.
2. Bryant, A. E., and Stevens, D. L. (2006) Clostridial toxins in the pathogenesis of gas gangrene, in The comprehensive sourcebook of bacterial protein toxins (Alouf, J. E., and Popoff, M. R., Eds.) pp 919−929, Academic Press, New York.
3. Awad, M. M., Bryant, A. E., Stevens, D. L., and Rood, J. I. (1995) Virulence studies on chromosomal alpha-toxin and theta-toxin mutants constructed by allelic exchange provide genetic evidence for the essential role of alpha-toxin in *Clostridium perfringens*-mediated gas gangrene. *Mol. Microbiol. 15*, 191–202.
4. Bunting, M., Lorant, D. E., Bryant, A. E., Zimmerman, G. A., McIntyre, T. M., Stevens, D. L., and Prescott, S. M. (1997) Alpha toxin from *Clostridium perfringens* induces proinflammatory changes in endothelial cells. *J. Clin. Invest. 100*, 565–574.
5. Ochi, S., Miyawaki, T., Matsuda, H., Oda, M., Nagahama, M., and Sakurai, J. (2002) *Clostridium perfringens* alpha-toxin induces rabbit neutrophil adhesion. *Microbiology 148*, 237–245.
6. Naylor, C. E., Eaton, J. T., Howells, A., Justin, N., Moss, D. S., Titball, R. W., and Basak, A. K. (1998) Structure of the key toxin in gas gangrene. *Nat. Struct. Biol. 5*, 738–746.
7. Tweten, R. K. (2005) Cholesterol-dependent cytolysins, a family of versatile pore-forming toxins. *Infect. Immun. 73*, 6199–6209.
8. Gilbert, R. J. (2010) Cholesterol-dependent cytolysins. *Adv. Exp. Med. Biol. 677*, 56–66.
9. Heuck, A. P., Moe, P. C., and Johnson, B. B. (2010) The cholesterol-dependent cytolysins family of Gram-positive bacterial toxins, in Cholesterol binding proteins and cholesterol transport (Harris, J. R., Ed.) pp 551−577, Springer, New York.
10. Heuck, A. P., Tweten, R. K., and Johnson, A. E. (2001) Beta-barrel pore-forming toxins: Intriguing dimorphic proteins. *Biochemistry 40*, 9065–9073.
11. Flanagan, J. J., Tweten, R. K., Johnson, A. E., and Heuck, A. P. (2009) Cholesterol exposure at the membrane surface is necessary and sufficient to trigger perfringolysin O binding. *Biochemistry 48*, 3977–3987.
12. Soltani, C. E., Hotze, E. M., Johnson, A. E., and Tweten, R. K. (2007) Structural elements of the cholesterol-dependent cytolysins that are responsible for their cholesterol-sensitive membrane interactions. *Proc. Natl. Acad. Sci. U.S.A. 104*, 20226–20231.
13. Soltani, C. E., Hotze, E. M., Johnson, A. E., and Tweten, R. K. (2007) Specific protein-membrane contacts are required for prepore and pore assembly by a cholesterol-dependent cytolysin. *J. Biol. Chem. 282*, 15709–15716.
14. Giddings, K. S., Johnson, A. E., and Tweten, R. K. (2003) Redefining cholesterol's role in the mechanism of the cholesterol-dependent cytolysins. *Proc. Natl. Acad. Sci. U.S.A. 100*, 11315–11320.
15. Ramachandran, R., Heuck, A. P., Tweten, R. K., and Johnson, A. E. (2002) Structural insights into the membrane-anchoring mechanism of a cholesterol-dependent cytolysin. *Nat. Struct. Mol. Biol. 9*, 823–827.
16. Heuck, A. P., Hotze, E. M., Tweten, R. K., and Johnson, A. E. (2000) Mechanism of membrane insertion of a multimeric β-barrel protein: Perfringolysin O creates a pore using ordered and coupled conformational changes. *Mol. Cell 6*, 1233–1242.
17. Hotze, E. M., Wilson-Kubalek, E. M., Rossjohn, J., Parker, M. W., Johnson, A. E., and Tweten, R. K. (2001) Arresting pore formation of a cholesterol-dependent cytolysin by disulfide trapping synchronizes the insertion of the transmembrane beta-sheet from a prepore intermediate. *J. Biol. Chem. 276*, 8261–8268.
18. Shepard, L. A., Shatursky, O., Johnson, A. E., and Tweten, R. K. (2000) The mechanism of pore assembly for a cholesterol-dependent cytolysin: Formation of a large prepore complex precedes the insertion of the transmembrane beta-hairpins. *Biochemistry 39*, 10284–10293.
19. Shatursky, O., Heuck, A. P., Shepard, L. A., Rossjohn, J., Parker, M. W., Johnson, A. E., and Tweten, R. K. (1999) The mechanism of membrane insertion for a cholesterol-dependent cytolysin: A novel paradigm for pore-forming toxins. *Cell 99*, 293–299.
20. Shepard, L. A., Heuck, A. P., Hamman, B. D., Rossjohn, J., Parker, M. W., Ryan, K. R., Johnson, A. E., and Tweten, R. K. (1998) Identification of a membrane-spanning domain of the thiol-activated pore-forming toxin *Clostridium perfringens* perfringolysin O: An alpha-helical to beta-sheet transition identified by fluorescence spectroscopy. *Biochemistry 37*, 14563–14574.
21. Czajkowsky, D. M., Hotze, E. M., Shao, Z., and Tweten, R. K. (2004) Vertical collapse of a cytolysin prepore moves its transmembrane beta-hairpins to the membrane. *EMBO J. 23*, 3206–3215.
22. Dang, T. X., Hotze, E. M., Rouiller, I., Tweten, R. K., and Wilson-Kubalek, E. M. (2005) Prepore to pore transition of a cholesterol-dependent cytolysin visualized by electron microscopy. *J. Struct. Biol. 150*, 100–108.
23. Farrand, A. J., LaChapelle, S., Hotze, E. M., Johnson, A. E., and Tweten, R. K. (2010) Only two amino acids are essential for cytolytic toxin recognition of cholesterol at the membrane surface. *Proc. Natl. Acad. Sci. U.S.A. 107*, 4341–4346.
24. Ramachandran, R., Tweten, R. K., and Johnson, A. E. (2004) Membrane-dependent conformational changes initiate cholesterol-dependent cytolysin oligomerization and intersubunit beta-strand alignment. *Nat. Struct. Mol. Biol. 11*, 697–705.
25. Awad, M. M., Ellemor, D. M., Boyd, R. L., Emmins, J. J., and Rood, J. I. (2001) Synergistic effects of alpha-toxin and perfringolysin O in *Clostridium perfringens*-mediated gas gangrene. *Infect. Immun. 69*, 7904–7910.
26. Heuck, A. P., and Johnson, A. E. (2005) Membrane recognition and pore formation by bacterial pore-forming toxins, in Protein-lipid interactions. From membrane domains to cellular networks (Tamm, L. K., Ed.) pp 163−186, Wiley-VCH, Weinheim.
27. Radhakrishnan, A., and McConnell, H. M. (1999) Condensed complexes of cholesterol and phospholipids. *Biophys. J. 77*, 1507–1517.
28. Huang, J., and Feigenson, G. W. (1999) A microscopic interaction model of maximum solubility of cholesterol in lipid bilayers. *Biophys. J. 76*, 2142–2157.
29. Heuck, A. P., Savva, C. G., Holzenburg, A., and Johnson, A. E. (2007) Conformational changes that effect oligomerization and initiate pore formation are triggered throughout perfringolysin O upon binding to cholesterol. *J. Biol. Chem. 282*, 22629–22637.
30. Nelson, L. D., Johnson, A. E., and London, E. (2008) How interaction of perfringolysin O with membranes is controlled by sterol structure, lipid structure, and physiological low pH: Insights into the origin of perfringolysin O-lipid raft interaction. *J. Biol. Chem. 283*, 4632–4642.
31. Moore, N. F., Patzer, E. J., Barenholz, Y., and Wagner, R. R. (1977) Effect of phospholipase C and cholesterol oxidase on membrane integrity, microviscosity, and infectivity of vesicular stomatitis virus. *Biochemistry 16*, 4708–4715.
32. Patzer, E. J., and Wagner, R. R. (1978) Cholesterol oxidase as a probe for studying membrane organisation. *Nature 274*, 394–395.
33. Ali, M. R., Cheng, K. H., and Huang, J. (2007) Assess the nature of cholesterol-lipid interactions through the chemical potential of cholesterol in phosphatidylcholine bilayers. *Proc. Natl. Acad. Sci. U.S.A. 104*, 5372–5377.
34. Ohvo, H., and Slotte, J. P. (1996) Cyclodextrin-mediated removal of sterols from monolayers: Effects of sterol structure and phospholipids on desorption rate. *Biochemistry 35*, 8018–8024.
35. Radhakrishnan, A., and McConnell, H. M. (2000) Chemical activity of cholesterol in membranes. *Biochemistry 39*, 8119–8124.
36. Leventis, R., and Silvius, J. R. (2001) Use of cyclodextrins to monitor transbilayer movement and differential lipid affinities of cholesterol. *Biophys. J. 81*, 2257–2267.
37. Lange, Y., and Steck, T. L. (2008) Cholesterol homeostasis and the escape tendency (activity) of plasma membrane cholesterol. *Prog. Lipid Res. 47*, 319–332.
38. Sokolov, A., and Radhakrishnan, A. (2010) Accessibility of cholesterol in endoplasmic reticulum (ER) membranes and activation of SREBP-2 switch abruptly at a common cholesterol threshold. *J. Biol. Chem. 285*, 29480−29490.
39. O'Brien, D. K., and Melville, S. B. (2000) The anaerobic pathogen *Clostridium perfringens* can escape the phagosome of macrophages under aerobic conditions. *Cell. Microbiol. 2*, 505–519.
40. O'Brien, D. K., and Melville, S. B. (2004) Effects of *Clostridium perfringens* alpha-toxin (PLC) and perfringolysin O (PFO) on cytotoxicity to macrophages, on escape from the phagosomes of macrophages, and on persistence of *C. perfringens* in host tissues. *Infect. Immun. 72*, 5204–5215.
41. Vazquez-Boland, J. A., Kuhn, M., Berche, P., Chakraborty, T., Dominguez-Bernal, G., Goebel, W., Gonzalez-Zorn, B., Wehland, J., and Kreft, J. (2001) *Listeria* pathogenesis and molecular virulence determinants. *Clin. Microbiol. Rev. 14*, 584–640.
42. Schnupf, P., and Portnoy, D. A. (2007) Listeriolysin O: A phagosome-specific lysin. *Microb. Infect. 9*, 1176–1187.
43. Heuck, A. P., Tweten, R. K., and Johnson, A. E. (2003) Assembly and topography of the prepore complex in cholesterol-dependent cytolysins. *J. Biol. Chem. 278*, 31218–31225.
44. Mayer, L. D., Hope, M. J., and Cullis, P. R. (1986) Vesicles of variable sizes produced by a rapid extrusion procedure. *Biochim. Biophys. Acta 858*, 161–168.
45. Ye, J., Esmon, N. L., Esmon, C. T., and Johnson, A. E. (1991) The active site of thrombin is altered upon binding to thrombomodulin: Two distinct structural changes are detected by fluorescence, but only one correlates with protein C activation. *J. Biol. Chem. 266*, 23016–23021.

46. Jameson, D. M., Croney, J. C., Moens, P. D. J., Gerard, Marriott, and Ian, P. (2003) Fluorescence: Basic concepts, practical aspects, and some anecdotes. *Methods Enzymol. 360*, 1–43.
47. Pace, C. N., and Scholtz, J. M. (1989) Measuring conformational stability of a protein, in Protein structure: A practical approach (Creighton, T. E., Ed.) pp 299−321, Oxford University Press, Oxford, U.K.
48. Bortoleto, R. K., de Oliveira, A. H., Ruller, R., Arni, R. K., and Ward, R. J. (1998) Tertiary structural changes of the alpha-hemolysin from *Staphylococcus aureus* on association with liposome membranes. *Arch. Biochem. Biophys. 351*, 47–52.
49. Santoro, M. M., and Bolen, D. W. (1988) Unfolding free energy changes determined by the linear extrapolation method. 1. Unfolding of phenylmethanesulfonyl alpha-chymotrypsin using different denaturants. *Biochemistry 27*, 8063–8068.
50. Pace, C. N. (1986) Determination and analysis of urea and guanidine hydrochloride denaturation curves. *Methods Enzymol. 131*, 266–280.
51. Tweten, R. K. (1988) Nucleotide sequence of the gene for perfringolysin O (theta-toxin) from *Clostridium perfringens*: Significant homology with the genes for streptolysin O and pneumolysin. *Infect. Immun. 56*, 3235–3240.
52. Tweten, R. K. (1988) Cloning and expression in *Escherichia coli* of the perfringolysin O (theta-toxin) gene from *Clostridium perfringens* and characterization of the gene product. *Infect. Immun. 56*, 3228–3234.
53. Rossjohn, J., Feil, S. C., McKinstry, W. J., Tweten, R. K., and Parker, M. W. (1997) Structure of a cholesterol-binding, thiol-activated cytolysin and a model of its membrane form. *Cell 89*, 685–692.
54. Lange, Y., Ye, J., Duban, M.-E., and Steck, T. L. (2009) Activation of membrane cholesterol by 63 amphipaths. *Biochemistry 48*, 8505–8515.
55. Ohno-Iwashita, Y., Iwamoto, M., Mitsui, K.-i., Ando, S., and Iwashita, S. (1991) A cytolysin, θ-toxin, preferentially binds to membrane cholesterol surrounded by phospholipids with 18-carbon hydrocarbon chains in cholesterol-rich region. *J. Biochem. (Tokyo) 110*, 369–375.
56. Zitzer, A., Bittman, R., Verbicky, C. A., Erukulla, R. K., Bhakdi, S., Weis, S., Valeva, A., and Palmer, M. (2001) Coupling of cholesterol and cone-shaped lipids in bilayers augments membrane permeabilization by the cholesterol-specific toxins streptolysin O and *Vibrio cholerae* cytolysin. *J. Biol. Chem. 276*, 14628–14633.
57. Clarke, J., and Fersht, A. R. (1993) Engineered disulfide bonds as probes of the folding pathway of barnase: Increasing the stability of proteins against the rate of denaturation. *Biochemistry 32*, 4322–4329.
58. Goni, F. M., and Alonso, A. (2000) Membrane fusion induced by phospholipase C and sphingomyelinases. *Biosci. Rep. 20*, 443–463.
59. Nieva, J. L., Goni, F. M., and Alonso, A. (1989) Liposome fusion catalytically induced by phospholipase C. *Biochemistry 28*, 7364–7367.
60. Takahashi, T., Sugahara, T., and Ohsaka, A. (1981) Phospholipase C from *Clostridium perfringens*. *Methods Enzymol. 7*, 710–725.
61. Palmer, M. (2004) Cholesterol and the activity of bacterial toxins. *FEMS Microbiol. Lett. 238*, 281–289.
62. Alouf, J. E., Billington, S. J., and Jost, B. H. (2006) Repertoire and general features of the family of cholesterol-dependent cytolysins, in The comprehensive sourcebook of bacterial protein toxins (Alouf, J. E., and Popoff, M. R., Eds.) pp 643−658, Academic Press, Oxford, England.
63. Ohno-Iwashita, Y., Iwamoto, M., Ando, S., and Iwashita, S. (1992) Effect of lipidic factors on membrane cholesterol topology—Mode of binding of θ-toxin to cholesterol in liposomes. *Biochim. Biophys. Acta 1109*, 81–90.
64. Lange, Y., Ye, J., and Steck, T. L. (2005) Activation of membrane cholesterol by displacement from phospholipids. *J. Biol. Chem. 280*, 36126–36131.
65. Alving, C. R., Habig, W. H., Urban, K. A., and Hardegree, M. C. (1979) Cholesterol-dependent tetanolysin damage to liposomes. *Biochim. Biophys. Acta 551*, 224–228.
66. Rosenqvist, E., Michaelsen, T. E., and Vistnes, A. I. (1980) Effect of streptolysin O and digitonin on egg lecithin/cholesterol vesicles. *Biochim. Biophys. Acta 600*, 91–102.
67. Bavdek, A., Gekara, N. O., Priselac, D., Gutierrez Aguirre, I., Darji, A., Chakraborty, T., Macˇek, P., Lakey, J. H., Weiss, S., and Anderluh, G. (2007) Sterol and pH interdependence in the binding, oligomerization, and pore formation of listeriolysin O. *Biochemistry 46*, 4425–4437.
68. Hotze, E. M., Heuck, A. P., Czajkowsky, D. M., Shao, Z., Johnson, A. E., and Tweten, R. K. (2002) Monomer-monomer interactions drive the prepore to pore conversion of a beta-barrel-forming cholesterol-dependent cytolysin. *J. Biol. Chem. 277*, 11597–11605.
69. Yeagle, P. L., and Young, J. E. (1986) Factors contributing to the distribution of cholesterol among phospholipid vesicles. *J. Biol. Chem. 261*, 8175–8181.
70. Veatch, S. L., and Keller, S. L. (2005) Miscibility phase diagrams of giant vesicles containing sphingomyelin. *Phys. Rev. Lett. 94*, 148101–148104.
71. Ziblat, R., Leiserowitz, L., and Addadi, L. (2010) Crystalline domain structure and cholesterol crystal nucleation in single hydrated DPPC: cholesterol:POPC bilayers. *J. Am. Chem. Soc. 132*, 9920–9927.
72. Jacobs, T., Cima-Cabal, M. D., Darji, A., Méndez, F. J., Vázquez, F., Jacobs, A. A. C., Shimada, Y., Ohno-Iwashita, Y., Weiss, S., and de los Toyos, J. R. (1999) The conserved undecapeptide shared by thiol-activated cytolysins is involved in membrane binding. *FEBS Lett. 459*, 463–466.
73. Polekhina, G., Feil, S. C., Tang, J., Rossjohn, J., Giddings, K. S., Tweten, R. K., and Parker, M. W. (2006) Comparative three-dimensional structure of cholesterol-dependent cytolysins, in The comprehensive sourcebook of bacterial protein toxins (Alouf, J. E., and Popoff, M. R., Eds.) pp 659−670, Academic Press, Oxford, England.
74. Pinkney, M., Beachey, E., and Kehoe, M. (1989) The thiol-activated toxin streptolysin O does not require a thiol group for cytolytic activity. *Infect. Immun. 57*, 2553–2558.
75. Saunders, F. K., Mitchell, T. J., Walker, J. A., Andrew, P. W., and Boulnois, G. J. (1989) Pneumolysin, the thiol-activated toxin of *Streptococcus pneumoniae*, does not require a thiol group for in vitro activity. *Infect. Immun. 57*, 2547–2552.
76. Korchev, Y. E., Bashford, C. L., Pederzolli, C., Pasternak, C. A., Morgan, P. J., Andrew, P. W., and Mitchell, T. J. (1998) A conserved tryptophan in pneumolysin is a determinant of the characteristics of channels formed pneumolysin in cells and planar lipid bilayers. *Biochem. J. 329*, 571–577.
77. Michel, E., Reich, K. A., Favier, R., Berche, P., and Cossart, P. (1990) Attenuated mutants of the intracellular bacterium *Listeria monocytogenes* obtained by single amino acid substitutions in listeriolysin O. *Mol. Microbiol. 4*, 2167–2178.
78. Stachowiak, R., Wisniewski, J., Osinska, O., and Bielecki, J. (2009) Contribution of cysteine residue to the properties of *Listeria monocytogenes* listeriolysin O. *Can. J. Microbiol. 55*, 1153–1159.
79. Cooper, R. A., Leslie, M. H., Fischkoff, S., Shinitzky, M., and Shattil, S. J. (1978) Factors influencing the lipid composition and fluidity of red cell membranes in vitro: Production of red cells possessing more than two cholesterols per phospholipid. *Biochemistry 17*, 327–331.
80. Jacobs, T., Darji, A., Frahm, N., Rohde, M., Wehland, J., Chakraborty, T., and Weiss, S. (1998) Listeriolysin O: Cholesterol inhibits cytolysis but not binding to cellular membranes. *Mol. Microbiol. 28*, 1081–1089.
81. Gaus, K., Rodriguez, M., Ruberu, K. R., Gelissen, I., Sloane, T. M., Kritharides, L., and Jessup, W. (2005) Domain-specific lipid distribution in macrophage plasma membranes. *J. Lipid Res. 46*, 1526–1538.
82. Harwood, C. R., and Cranenburgh, R. (2008) *Bacillus* protein secretion: An unfolding story. *Trends Microbiol. 16*, 73–79.
83. Rafii, F., Park, M., Bryant, A. E., Johnson, S. J., and Wagner, R. D. (2007) Enhanced production of phospholipase C and perfringolysin O (alpha and theta toxins) in a gatifloxacin-resistant strain of *Clostridium perfringens*. *Antimicrob. Agents Chemother. 52*, 895–900.
84. Hamman, B. D., Hendershot, L. M., and Johnson, A. E. (1998) BiP maintains the permeability barrier of the ER membrane by sealing the lumenal end of the translocon pore before and early in translocation. *Cell 92*, 747–758.
85. Urbina, P., Flores-Díaz, M., Alape-Girón, A., Alonso, A., and Goni, F. M. (2009) Phospholipase C and sphingomyelinase activities of the *Clostridium perfringens* α-toxin. *Chem. Phys. Lipids 159*, 51–57.
86. Goldfine, H., Knob, C., Alford, D., and Bentz, J. (1995) Membrane permeabilization by *Listeria monocytogenes* phosphatidylinositol-specific phospholipase C is independent of phospholipid hydrolysis and cooperative with listeriolysin O. *Proc. Natl. Acad. Sci. U.S.A. 92*, 2979–2983.
87. Smith, G. A., Marquis, H., Jones, S., Johnston, N. C., Portnoy, D. A., and Goldfine, H. (1995) The two distinct phospholipases C of *Listeria monocytogenes* have overlapping roles in escape from a vacuole and cell-to-cell spread. *Infect. Immun. 63*, 4231–4237.
88. Birmingham, C. L., Canadien, V., Kaniuk, N. A., Steinberg, B. E., Higgins, D. E., and Brumell, J. H. (2008) Listeriolysin O allows *Listeria monocytogenes* replication in macrophage vacuoles. *Nature 451*, 350–354.
89. Alberti-Segui, C., Goeden, K. R., and Higgins, D. E. (2007) Differential function of *Listeria monocytogenes* listeriolysin O and phospholipases C in vacuolar dissolution following cell-to-cell spread. *Cell. Microbiol. 9*, 179–195.
90. Barlic, A., Gutierrez-Aguirre, I., Caaveiro, J. M., Cruz, A., Ruiz-Arguello, M. B., Perez-Gil, J., and Gonzalez-Manas, J. M. (2004) Lipid phase coexistence favors membrane insertion of equinatoxin-II, a pore-forming toxin from *Actinia equina*. *J. Biol. Chem. 279*, 34209–34216.